Journal of Physics: Conference Series **308** (2011) 012025 doi:10.1088/1742-6596/308/1/012025

Monitoring the parameters of a large size liquid Argon Time Projection Chamber using UV laser beams

Biagio Rossi
on behalf of LHEP liquid Argon group

Albert Einstein Center for Fundamental Physics, Laboratory for High Energy Physics (LHEP), University of Bern, Switzerland

E-mail: biagio.rossi@lhep.unibe.ch

Abstract. This paper reports on multiphoton ionization at 266 nm of liquid Argon in a Time Projection Chamber (LAr TPC) detector. The electron signal produced by the laser beam is a formidable tool for the monitoring of the next generation large mass LAr TPCs [1]. The detector we have designed and tested allowed us also to measure the two-photon absorption cross-section (σ_{ex}) of LAr with unprecedented accuracy and precision, appropriate for using the UV laser technique also for a quantitative calibration of the detector.

1. Introduction

The liquid Argon Time Projection Chamber (LAr TPC) detector technology allows for uniform and high resolution imaging of massive detector volumes. The operating principle of the LAr TPC is based on the undistorted transport of tracks of ionizing electrons in highly purified LAr by a uniform electric field over distances up to a few metres. Imaging is provided by wire planes or other read-out devices placed at the end of the drift path. The drifting electrons are collected by the outermost wire plane which gives position and calorimetric information. Additional planes with different orientation can be positioned in front of the collection plane to record the signal induced by the passage of the drifting electrons. This provides different projective views of the same event thus allowing space point reconstruction. The third coordinate is given by the measurements of the drift time given by the time interval between the passage of the ionizing particle in the active volume (t_0) and the arrival of the drifting electrons on the wire planes. The t_0 can come from the detection of the scintillation light of liquid Argon by means of photomultipliers, or from an external source. The particle momentum of an incoming particle is inferred by the measurement of its multiple scattering [2], while the detection of the local energy deposition provides particle identification. For more information, the reader is referred to [1] and references therein quoted.

A very large LAr TPC with a mass ranging from 10 kton to 100 kton would produce an important physics output thanks to the excellent event reconstruction performance [3, 4, 5, 6, 7]. The purity of the liquid Argon is a key ingredient to achieve imaging over long drift distances (>5 m), needed for building such a large masses. In particular, a purity corresponding to less than 0.1 ppb of electronegative elements such as Oxygen, has to be achieved in order to allow

for electron lifetimes of milliseconds and, hence, drift distances of meters. Moreover, the purity of LAr has to be monitored continuously while TPC is running, thus calling for practical and efficient purity monitoring techniques.

To this end, laser based methods are very interesting as they provide a reliable route to tackle the problem. In addition, a laser beam is an ideal tool for perforimg the energy calibration of the detector, for measuring the drift velocity, the space and time resolution of the detector, the capability of double track separation, the diffusion of the drifting electrons, and also for verifing the homogeneity of the drift field. Furthermore, the laser technique can be also used in the *double phase* LAr TPCs [3, 8] for the monitoring of the stability of the read-out amplification stages.

In this paper, the UV laser multiphoton ionization of liquid Argon with the 4^{th} harmonic of a Nd-YAG laser is illustrated. In the first part, the monitoring of the parameters of a LAr TPC with laser beams is pointed out. In the second part, a theoretical introduction to the multiphoton ionization with an accurate measurement of the two-photon absorption cross section of LAr (σ_{ex}), which is the atomic intermediate step to ionization, fundamental for reliable calibration of LAr TPCs, is presented.

The interaction of laser light with liquid matter is comparatively less studied with respect to gas and solid phase. Nevertheless, some important features are well understood [9]. Laser ionization can occur as a multiphoton process through the simultaneous absorption of two or more photons via virtual states in a medium. This process requires high photons flux, namely, pulsed lasers. In a multiphoton process, bound electrons absorb several laser photons simultaneously, thus exciting the atom to high energy levels or even to ionization.

The measurements described in this paper are done with a prototype LAr TPC described in [1] that is part of a R&D project we are conducing in Bern envisioning the realization of LAr TPC detectors of increasing size. First results have been published also on the study of a TPC we have built and operated employing a mixture of LAr and Nitrogen [10].

2. Experimental setup

The detector (figure 1) used for the measurements consists of a TPC (figure 2) housed in a tube filled with purified liquid Argon, in thermal contact with a bath of liquid Argon (figure 3). The TPC is complemented by an electronic read-out and data acquisition system (DAQ), a liquid Argon recirculation and purification system, a photomultiplier (PMT), a series of ancillary equipments for monitoring and control, and a UV-laser with the related optics to allow the study of multiphoton ionization of liquid Argon.

The TPC detector is contained in a stainless-steel cylindrical tube. The latter measures 50 cm in diametre and 110 cm in height, for an inner volume of about 200 litres. The tube is placed in thermal contact with a bath of liquid Argon and is closed by a stainless-steel flange. A series of additional smaller flanges are positioned on the top flange. They include feed-throughs needed to evacuate the inner volume of the vessel, to fill it with liquid Argon, to read-out the detector signals, to supply the high-voltage, to house the pressure monitors, level metre and safety valves, and to provide the transport of the UV laser beams to the inner part of the TPC. The various components are described in detail in [1].

Figure 4 shows the arrangement and the path of the laser beam used for the measurements. The laser beam passes through a system of prisms to be *cleaned* from the residuals of the 1^{st} and 2^{nd} harmonic components. After a deflection on a 266 nm coated mirror, it is then fed in a variable, motorized attenuator. After the attenuator two parallel beams of variable intensity are present. One is dumped, while the other is used for the measurements. The use of the attenuator is important, as it allows to vary the energy of the laser beam without changing the laser generation parameters. Consequently, the laser shows better stability performance. Both energy and pulse length measurements are performed before the beam is finally steered into the

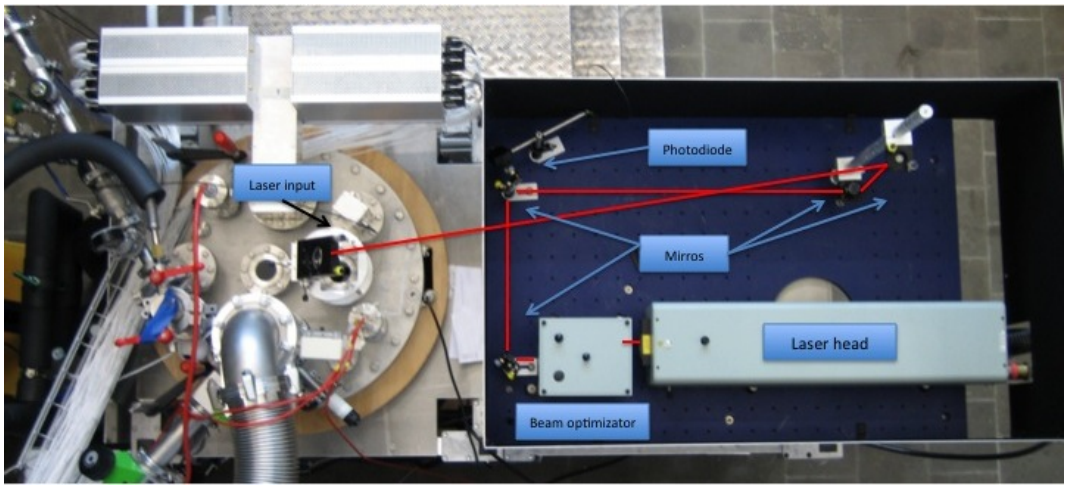

Figure 1. Photograph of the experimental setup (top view) including the laser beam. Red lines show the beam path before being steered into the detector.

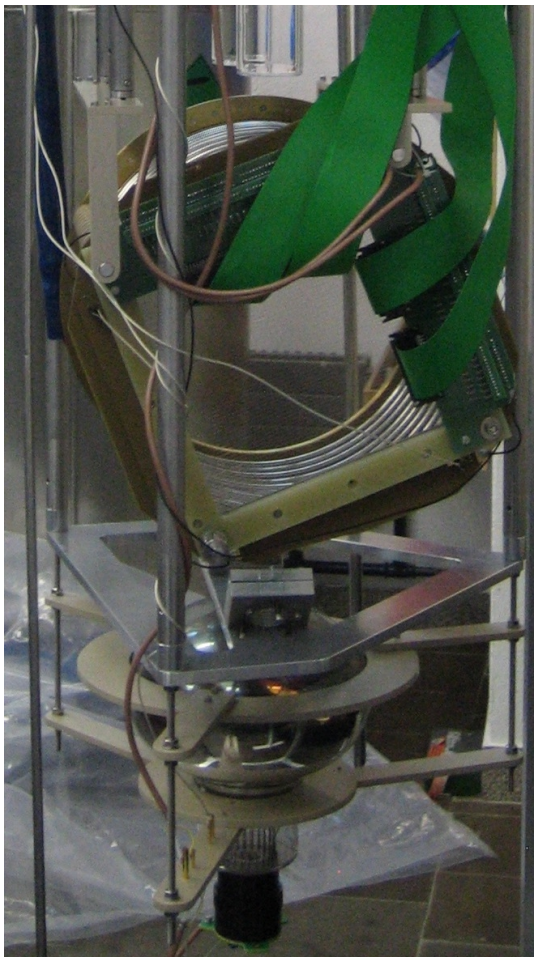

Figure 2. Photograph of the experimental setup. The TPC, the PMT and a mirror installed on a stainless steel support are clearly visible. The drift direction is horizontal with induction (collection) wires running at an angle of 25 degrees relative to the vertical (horizontal) direction.

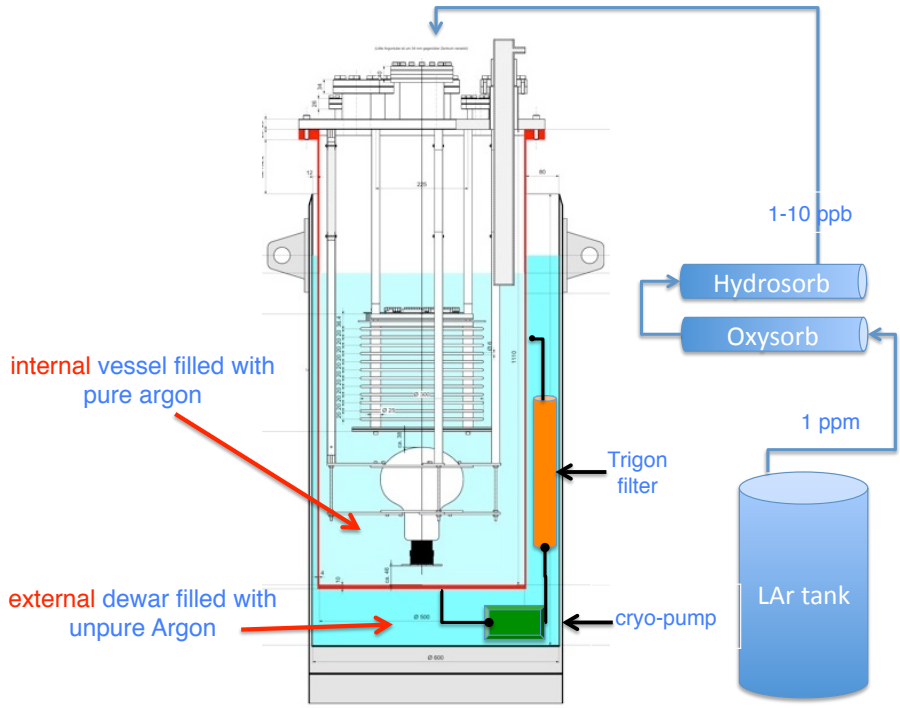

Figure 3. Schematic drawing of the detector set-up. The TPC, mounted with the drift coordinate vertically. The PMT and the relative supports are housed in a cylindrical tube filled with pure Argon. The external vessel that contains un-purified Argon hosts the liquid purification/recirculation system.

chamber.

In theoretical calculations (section 5.2), we assume for simplicity that the transverse distribution of the laser intensity has a square shape. In the experiment, the laser beam passes after the attenuator through a diaphragm of 4 mm diameter selecting the more uniform, central part of the beam. In this way one obtains a definite beam cross section also preventing any effect of the laser beam tails (halo) on the ionization process. In fact, the contribution to ionization of photons in the halo is negligible due to the nonlinear character of the process.

After the diaphragm, the light is fed into the TPC inner volume by passing through a system of mirrors (figure 1) and a custom made optical feedthrough [1].

As described in figure 4, the beam passes two times in the active volume, thus producing a vertical track orthogonal to the drift coordinate and a second track *inclined* with respect to the drift coordinate. After the second passage, the beam is steered out of the dewar by means of another optical feedthrough. The extraction of the laser beam from the TPC allows for the monitoring of its energy, after ionization of LAr has occurred. Cross check of the energy measurements at the entrance and exit optical feedthroughs indicates no depletion of the ionizing laser beam.

The measurement of the pulse width is performed by means of a fast photodiode[1], calibrated in energy with an energy meter[2] and readout by a CAEN V1729 ADC. The board, a Switched-Capacitor Digitizer, performs the coding of 4 analog channels of bandwidth up to 300 MHz over 12 bits at a sampling frequency of up to 2 GS/s and over a depth of 2520 usable points. It is suited for acquisition of fast analog signals.

[1] Thorlabs DET 10 A.
[2] GEANTEC - SOLO 2.

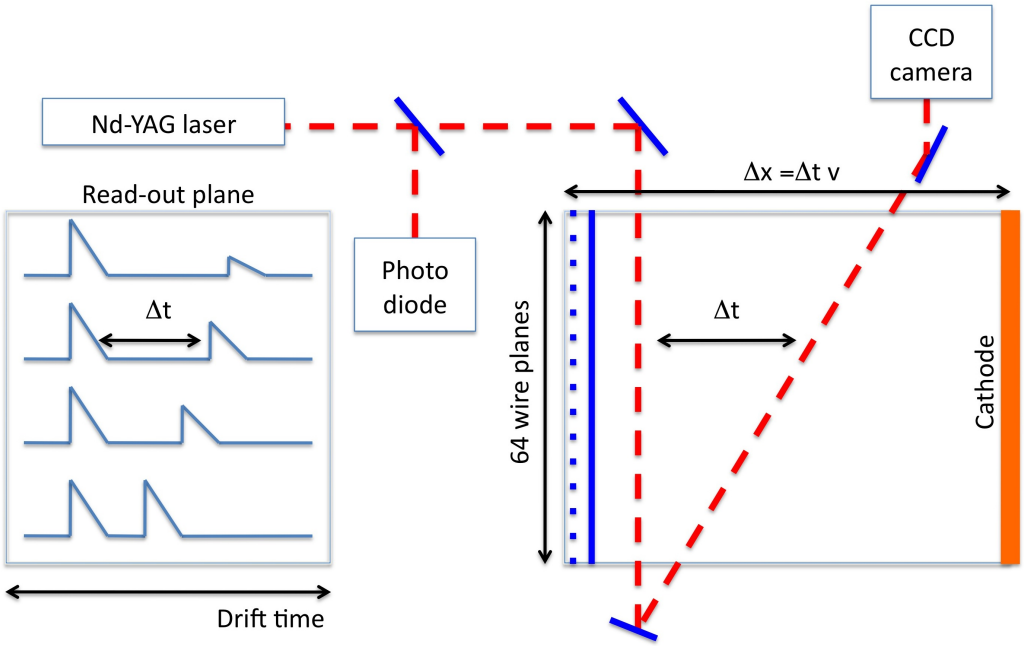

Figure 4. Schematic view of the laser beam path and the readout response.

3. Detector operation and data taking

Before filling with liquid Argon, the detector vessel is evacuated to a residual pressure of 10^{-5} mbar. The detector is then filled with ultra pure liquid Argon flown through the purification cartridges in liquid phase, analogous to the purification unit inserted in the recirculation system. The purity of the liquid Argon before passing through the OXYSORB [11] cartridge has a nominal concentration of water and Oxygen of the order of a ppm. The procedure is described in details in [1]

Several measurements were performed with the TPC installed with the electrons drifting along the horizontal direction. The detection of the first UV laser induced ionization tracks have been published in [1].

In figure 5 the display of a typical UV laser induced event is shown. Two tracks along all the wires at different drift time are well visible. The beam first generates the same signal over all the wires of the TPC collection plane at the same time (drift coordinate), and then, after the reflection on a mirror the beam passes through the active volume again inducing a second track *inclined* with respect to the drift coordinate. In figure 6 typical waveform peaks induced by a single UV laser pulse on a collection wire are shown. Two peaks at different drift time are clearly visible.

4. Monitoring drift velocity and LAr purity

The drift velocity is determined knowing *a priori* the distance between the two tracks, and measuring the difference between the drift time of the peaks (wire by wire) induced by the tracks.

In figure 7 the velocity of the drifting electrons as a function of the drift field intensity is shown. We performed two campaigns of measurements, collecting for each 1000 UV laser-induced events, for different values of the drift field. Results, for different LAr temperatures, are listed in the column of table 1. For the same field intensity, the higher the temperature, the lower

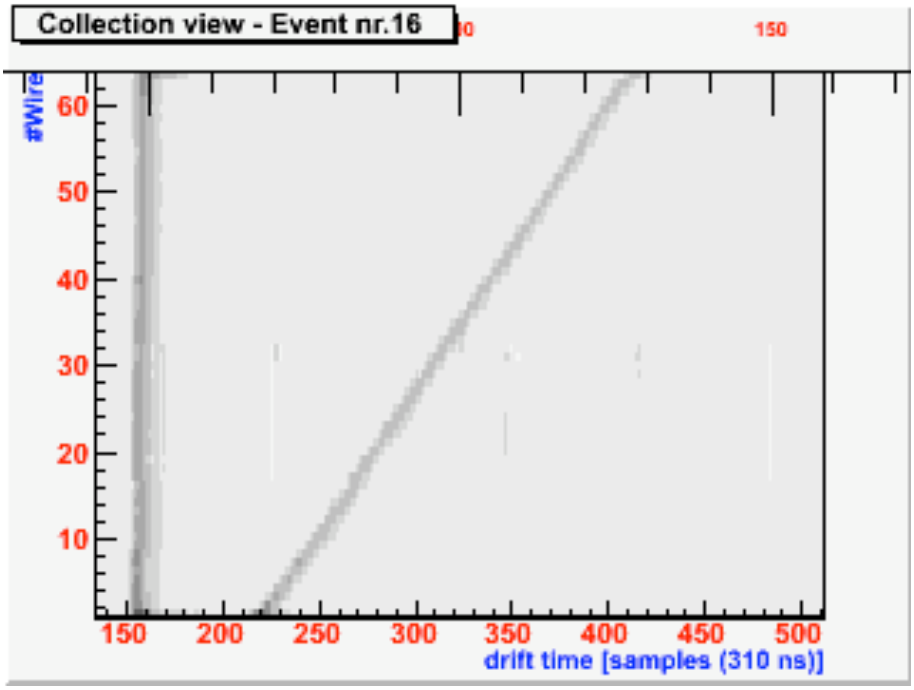

Figure 5. Event display of a UV laser ionization event in the setup described above. Two tracks along all the wires at different drift time are visible. The beam first generates the same signal over all the wires of the collection plane at the same time (drift coordinate) and then after the reflection on a mirror passes through the active volume again indcucing another track *inclined* with respect to the drift coordinate.

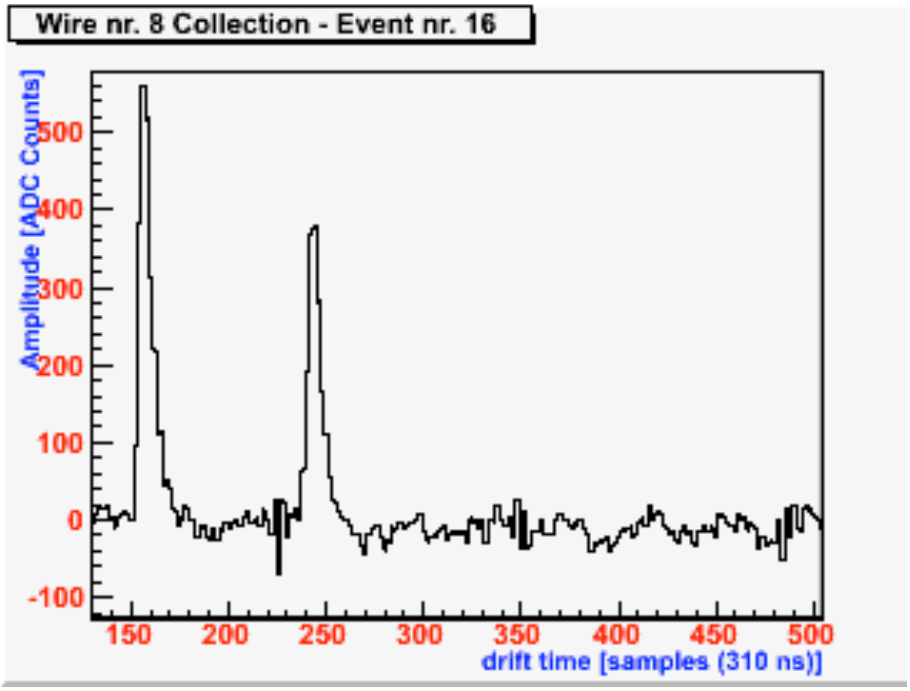

Figure 6. Typical signals induced on a wire of the TPC collection plane by the two UV laser induced tracks. Two peaks at different drift time are clearly visible. The area under each peak provides the electron yield.

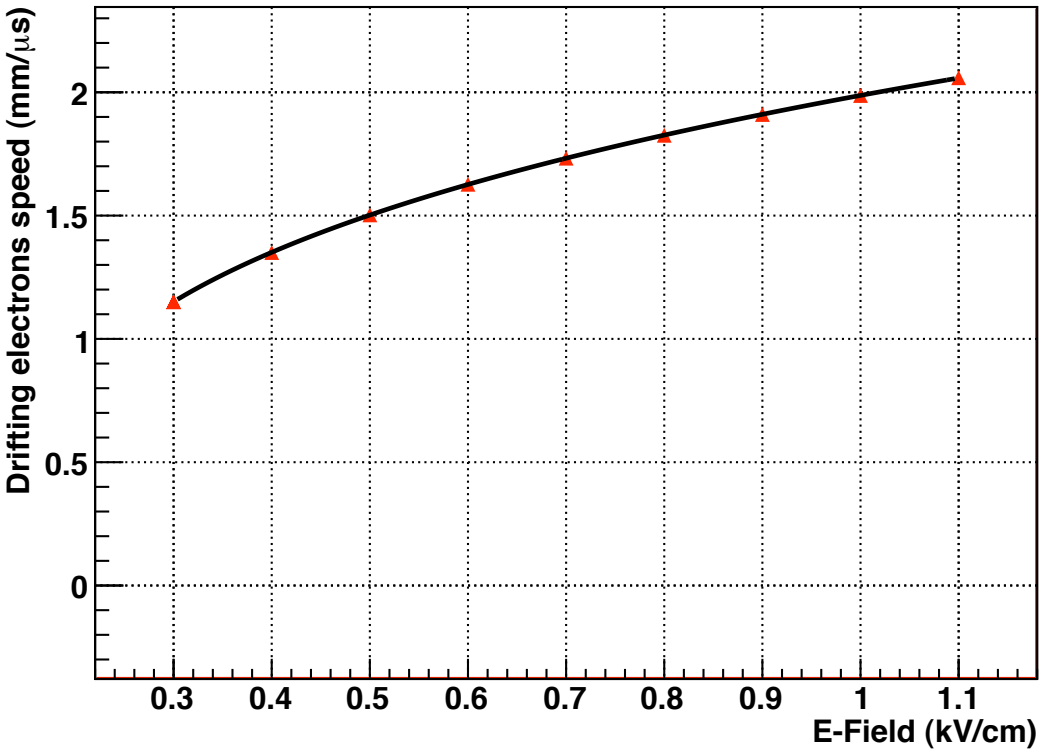

Figure 7. Drifting electrons lifetime (μs) as a function of the electric field intensity (T=89.1 K). The error bars are smaller than the points. The fit was performed with an empirical formula taken from [12, 13].

is the drift velocity. Data well agree with the theoretical predictions and with previous results [12, 13, 14].

Table 1. Velocity of drifting electrons for different electric fields.

E (kV/cm)	v (mm/μs)@88.9 K	v (mm/μs)@89.1 K
1.20	2.138 ± 0.006	
1.10	2.089 ± 0.006	2.059 ± 0.006
1.00	2.021 ± 0.006	1.987 ± 0.006
0.90	1.943 ± 0.006	1.910 ± 0.005
0.80	1.857 ± 0.005	1.826 ± 0.005
0.70	1.759 ± 0.005	1.738 ± 0.005
0.60	1.656 ± 0.004	1.627 ± 0.008
0.50	1.530 ± 0.004	1.503 ± 0.004
0.40	1.371 ± 0.003	1.350 ± 0.004
0.30	1.158 ± 0.004	1.150 ± 0.005
0.20	0.883 ± 0.004	

The electrons attachment to the electronegative impurities present in the LAr during the drift diminish the charge collected by the wire planes. The measurement of the charge attenuation along the drift time provides an estimate of the LAr purity. In figure 8 the profile histogram of the charge produced by 1000 *inclined* laser tracks as a function of the drift field is shown.

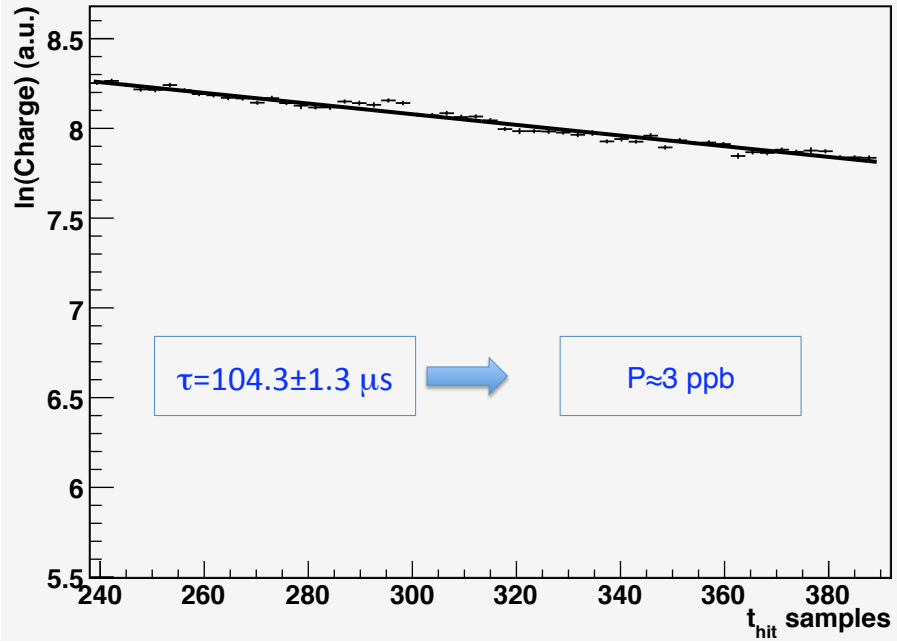

Figure 8. Profile histogram of the charge induced by 1000 laser tracks as a function of the drift time. The points are fit with line $f(t) = q_0 - (t_{hit} - t_0)/\tau$, where q_0 is the charge produced by the laser track, t_0 is the position (along the abscissa) of the wire planes, t_{hit} is the drift coordinate, and τ is the drifting electrons lifetime in LAr. For this sample of data $\tau = (104.3 \pm 1.3)$ μs.

The points on the figures were fit with a line $f(t) = q_0 - (t_{hit} - t_0)/\tau$, where q_0 is the charge produced by the laser track, t_0 is the position (along the abscissa) of the wire planes, t_{hit} is the drift coordinate, and τ is the drifting electrons lifetime in LAr. The τ is related to the purity via the following formula:

$$\mathrm{P[ppb]} \sim \frac{300}{\tau[\mu\mathrm{s}]} \tag{1}$$

The fit yields a lifetime of $\tau = 104.3 \pm 1.3$ μs and, hence, a purity of about 3 ppb of O_2 eq.

5. Multiphoton absorption of LAr

An atom with ionization energy E_i can be ionized by irradiation with photons with energy $E=h\nu$ much lower than E_i if the photon flux is intense enough to promote multiphoton absorption.

One of the features of multiphoton absorption is that it can occur via laser-induced virtual states, which are not eigenstates of the atom. Thus, it does not require any intermediate atomic state. These laser induced virtual states are characterized by a lifetime $\tau^{virtual}$ of the order of one optical cycle. For the laser used in the present experiment we have:

$$\tau^{\mathrm{virtual}}_{266\ \mathrm{nm}} \approx \frac{\lambda}{2\pi c} \approx 1.4 \cdot 10^{-16}\ \mathrm{s} \tag{2}$$

while the lifetime of an intermediate (excited) *real* state is of the order of $\tau \sim 10^{-8}$ s [15]. When an atomic state is located not too far from a laser-induced virtual state (quasi-resonant ionization), the multiphoton absorption process is stronlgy enhanced, thus requiring a laser intensity much lower than in the non-resonant case [15].

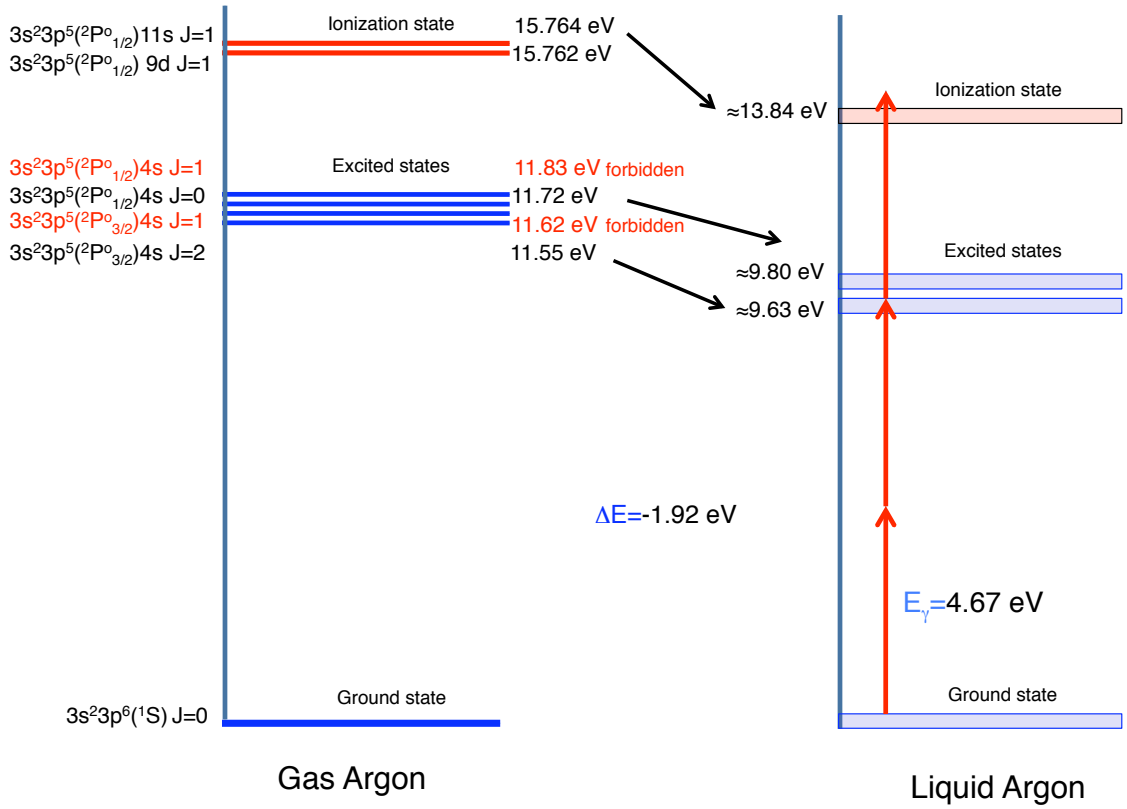

Figure 9. Schematics of the gas/liquid Argon energetic levels. In the passage from gas to liquid phase, the absolute values of the energetic levels of the atom are reduced [9] and the lines broaden, becoming energy bands as in the condensed matter.

5.1. Energy levels in liquid Argon

The interaction of laser light with matter in the liquid phase has been comparatively less studied with respect to gas and solid phase. Nevertheless, some important features are well understood [9]. In the passage from gas to liquid phase, the energy separation between the energy levels reduces. This is sketched in figure 9 where the energy levels of gas and liquid Argon are compared. The ionization potential for Argon gas (GAr) is $I_p = 15.76$ eV [16], and four excited states potentially involved in a multiphoton process lie at 11.83 eV, 11.72 eV, 11.62 eV and 11.55 eV, respectively. For two-photon absorption $\Delta J = 0, 2$ and, hence, only the transitions to levels with J=0 and J=2 are allowed by conservation rules. The effects leading to the energy shift can be summarized in the following formula [17]:

$$I_p^{\text{liquid}} = I_p^{\text{gas}} + P_+ + V_0 \tag{3}$$

where I_p^{gas} (I_p^{liquid}) is the ionization potential in gas (liquid) phase and V_0 is the energy of the quasi-free electron at the bottom of the conduction band of the liquid. The polarization energy P_+ of the positive ion is given by the Born equation [18]:

$$P_+ = -\frac{e^2}{2r_+}(1 - \epsilon^{-1}) \tag{4}$$

In the classical approximation, a liquid is treated as a uniform continuum with the optical dielectric constant ϵ, while a positive ion is regarded as a sphere with radius r_+ and charge e.

For Argon the values experimentally measured are ϵ=1.5 at 550 nm and ϵ=1.9 at 128 nm, but an extrapolation from a plot published in [19] leads to ϵ=1.59 at 266 nm. Since $V_0 = -0.17$ eV [20], $r_+ = 0.088$ nm, we have $P_+ = -1.75$ eV thereby the ionization state in liquid turns out to be $I_p^{\rm liquid} = I_p^{\rm gas} - 1.92$ eV. Consequently, the ionization and the lowest excited state energies become, respectively:

$$I_p^{\rm liquid} = 13.84 \text{ eV} \quad , \quad I_e^{\rm liquid} = 9.63 \text{ eV} \tag{5}$$

in our experiment we have used the 4$^{\rm th}$ harmonic (λ=266 nm, corresponding to a photon energy of 4.67 eV) of a Nd-YAG laser source, the main features of which are reported in Table 2.

Table 2. 4$^{\rm th}$ harmonic UV laser specifications (Continuum, model Surelite I-10)

wavelength (nm)	max rep. rate (Hz)	max energy (mJ)	energy stability
266	10	82	5%
pulse width (ns)	rod diameter (mm)	divergence (mrad)	FWHM (ns)
5-7	6	0.6	5.7

At this wavelength at least three photons are needed to produce ionization in LAr, although the intermediate *real* state can make the actual multiphoton transition a 2+1 transition. In fact, the lowest allowed excited state lies at 9.63 eV, which is only 0.3 eV higher than the energy of two photons at 266 nm. However, it is very plausible that this energy gap disappears in the liquid phase due to band formation and the consequent level broadening of the atomic energy levels [9].

5.2. Rate equations

In a multiphoton ionization process the N-photon ionization rate W is given by $W = \sigma_N F^N$, where σ_N is the generalized N-photon ionization cross-section. The rate W is expressed in reciprocal seconds, σ_N is expressed in cm^{2N} s^{N-1} and the laser flux F is in photon cm^{-2} s^{-1}.

For gases the one-photon absorption cross-section σ_1 is typically of the order of 10^{-17}cm^2[21], whereas the two-photon and the three-photon cross-sections are of the order of $\sigma_2 = W/F^2 \sim 10^{-50}$cm^{4}s and $\sigma_3 = W/F^3 \sim 10^{-83}$cm^{6}s^2, respectively.

From the energy levels depicted in figure 9 we can write the following rate equation to retrieve the expected rate of excited electrons produced:

$$\frac{dN_{ex}}{dt} = (N_0 - N_{ex})F^2\sigma_{ex} - N_{ex}\sigma_i F - N_{ex}/\tau \tag{6}$$

where N_0 is the initial density of atoms in the ground state, N_{ex} the density of atoms in the excited state, σ_{ex} the two-photon transition cross-section from ground to the intermediate excited state, σ_i is the single photon transition cross-section from the excited state to the continuum, and τ the lifetime of the excited state, respectively. The rate of ionization is given by:

$$\frac{dN_i}{dt} = N_{ex}\sigma_i F \tag{7}$$

where N_i is the density of ionized atoms (or number of extracted electrons). Here we consider the ion/electron recombination negligible for UV laser induced events at our operational drift field [22]. Defining $h = \sigma_{ex}F^2 + \sigma_i F + \frac{1}{\tau}$, replacing equation (6) in equation (7) and time-integrating ($dt = s$) one obtains:

$$N_i = \frac{N_0\sigma_i\sigma_{ex}F^3}{h}\Big(\frac{e^{-hs}-1}{h} + s\Big) \tag{8}$$

where s is the FWHM of the laser pulse (in our case s=$(5.7 \pm 5\%) \cdot 10^{-9}$ s).

Three different regions can be defined:

- low photon flux for $hs << 1$;
- high photon flux for $hs >> 1$, $\sigma_{ex}F^2 << \sigma_i F$ and $1/\tau << \sigma_i F$;
- very high photon flux for $hs >> 1$, $\sigma_{ex}F^2 >> \sigma_i F$ and $1/\tau << \sigma_{ex}F^2$.

In the region of low photon flux equation (8) can be written as:

$$N_i = \frac{1}{2} N_0 \sigma_{ex} \sigma_i s^2 F^3 \tag{9}$$

showing a cubic dependence of the density of the electrons in the ionized state with respect to the flux of photons. In the high photon flux regime equation (8) becomes:

$$N_i = N_0 \sigma_{ex} s F^2 \tag{10}$$

exibiting a quadratic dependence. Finally, for very high photon flux equation (8) can be approximated as:

$$N_i = N_0 \sigma_i s F \tag{11}$$

with a linear dependence due to the saturation of the two-photon transition.

6. Measurement of the two photon absorption cross section

In order to estimate the cross-sections σ_{ex} and σ_i of the rate equations presented above, and the lifetime of the excited state of LAr, we measured the rate of electrons produced by the laser beam as a function of the photon flux. For each laser track we determined the total electron yield produced by the laser (for each wire) simultaneously, monitoring pulse-by-pulse the energy, and FWHM of the beam. For the data set shown below, the beam energy was varied in the range 0.1÷2.0 mJ.

Figure 10 reports the rate of electrons (measured in electron atom^{-1} s^{-1}) as a function of the photon flux (measured in photon cm^{-2} s^{-1}), in a log-log plot. In the investigated intensity range the data are well described by a straight line, and the experimental points are very well fitted with a power law dependence on photon flux F (see equation 9-11). In particular, the best fit is obtained by using equation 10 in the following form:

$$\frac{N_{ex}}{N_0 s} = \sigma_{ex} \cdot F^n \tag{12}$$

with n and σ_{ex} as free parameters. The corresponding best fitted values are:

$$n = 2.02 \pm 0.05 \tag{13}$$

$$\sigma_{ex} = (1.24 \pm 0.10_{\text{stat}} \pm 0.30_{\text{syst}}) \cdot 10^{-56} \text{ cm}^4\text{s} \tag{14}$$

The value of n is consistent with 2, indicating that at our laser intensities the limiting step of the three-photon ionization process is the two-photon absorption to the intermediate state.

The value of σ_{ex} presented here provides a reliable and accurate measurements of the two-photon absorption cross section of LAr [22]. It is within the range of the two-photon absorption cross-section for liquids [23, 24]. The assumption made ($hs >> 1$, $\frac{1}{\tau} << \sigma_i F$ and $\sigma_i F >> \sigma_{ex} F^2$) to approximate equation (8) to equation (10) are justified by the experimental data. Moreover, the results are well consistent with the values $\sigma_i = 10^{-16}$-10^{-17} cm^2 and $\tau = 10^{-7}$-10^{-8} s provided by [21, 25, 26].

Systematic uncertainties due to the absolute energy calibration of the TPC and to the measurement of the photon flux have been evaluated. We assume a 25% uncertainty on the absolute number of electrons collected, and 10% uncertainty on the pulse-by-pulse measurement of the beam energy.

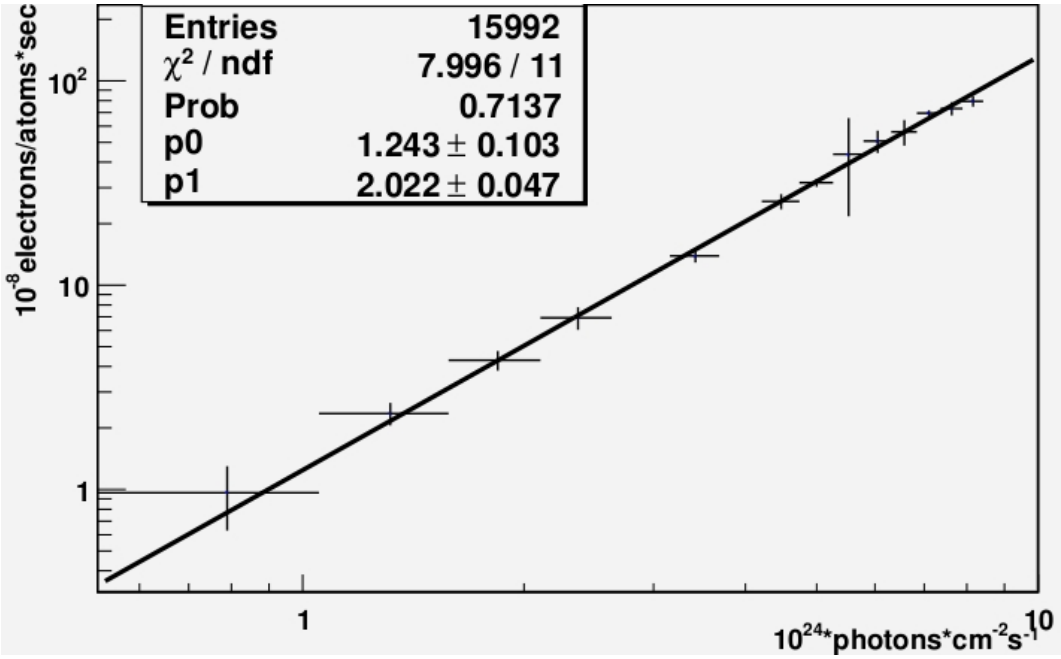

Figure 10. Profile histogram of the rate of electrons as a function of the photon flux of the laser beam.

7. Conclusions and outlook

We reported on the measurement of UV laser-induced multiphoton ionization of LAr performed with a liquid Argon Time Projection Chamber detector. The possibility of using such a technique for the general monitoring of the parameters (i.e. measurements of LAr purity) of LAr TPC detectors of large size has been shown. Furthermore, for the first time, the value of the two-photon absorption cross-section $\sigma_{ex} = (1.24 \pm 0.10_{\rm stat} \pm 0.30_{\rm syst}) \cdot 10^{-56}$ cm^{4}s has been determined with a good accuracy appropriate for quantitative calibration of LAr TPC detectors.

The results obtained and described in this paper make us confident on the practical use of UV laser beams technique for the general monitoring and for the calibration of LAr TPC detectors, as requested for the envisioned large scale applications of the technique.

Acknowledgements

The work presented in this paper was conducted thanks to grants from the Swiss National Science Foundation (SNF) and from the University of Bern. We warmly acknowledge both institutions. We wish to warmly thank our technical collaborators R. Haenni, P. Lutz and F. Nydegger, for their skillful help in building and operating the detector and the related infrastructure.

References

[1] B. Rossi *et al.*, A prototype liquid Argon Time Projection Chamber for the study of UV laser multi-photonic ionization, JINST **4** (2009) P07011.
[2] A. Ankowski *et al.*, Measurement of through-going particle momentum by means of multiple scattering with the ICARUS T600 TPC, Eur. Phys. J. C 48 (2006) 667.
[3] D. Autiero *et al.*, Large underground, liquid based detectors for astro-particle physics in Europe: scientific case and prospects, JCAP 0711:011 (2007).
[4] A. Ereditato and A. Rubbia, Ideas for future liquid Argon detectors, Nucl. Phys. Proc. Suppl. 139 (2005) 301.
[5] A. Ereditato and A. Rubbia, The liquid Argon TPC: a powerful detector for future neutrino experiments and proton decay searches, Nucl. Phys. Proc. Suppl. 154 (2006) 163.

[6] A. Ereditato and A. Rubbia, Conceptual design of a scalable multi-kton superconducting magnetized liquid Argon TPC, Nucl. Phys. Proc. Suppl. 155 (2006) 233.
[7] B. Baibussinov *et al.*, A new, very massive modular Liquid Argon Imaging Chamber to detect low energy off-axis neutrinos from the CNGS beam. (Project MODULAr), arXiv:0704.1422.
[8] A. Badertscher *et al.*, Construction and operation of a Double Phase LAr Large Electron Multiplier Time Projection Chamber, arXiv:0811.3384, (2008).
[9] W.F. Schmidt, Electronic Conduction Processes in Dielectric Liquids, IEEE Trans. Electrical Insulation EI-19 (1984) 389.
[10] A. Ereditato *et al.*, Study of ionization signals in a TPC filled with a mixture of liquid Argon and Nitrogen, JINST **3** (2008) P10002.
[11] Messer Schweiz AG, http://www.messer.ch
[12] A.M.Kalinin *et al.*, ATLAS Internal Note, ATLAS-LARG-NO-058, (1996) CERN.
[13] W. Walkowiak, Drift velocity of free electrons in liquid argon, Nucl. Instr. Meth. in Phys. Res. **A449** (2000) 288.
[14] S. Amoruso *et al.*, Analysis of the liquid argon purity in the ICARUS T600 TPC, Nucl. Instr. Meth. in Phys. Res. **A516** (2004) 68.
[15] S.L Chin and P.Lambropoulos, Multiphoton ionization of Atoms, Academic Press Canada (1984).
[16] NIST - National Institute of Standards and Technology, NIST Chemstry WebBook, NIST Standard Reference Databse N. 69.
[17] B. Raz and J. Jortner, Energy of the quasi-free electron state in liquid and solid rare gases, Chem. Phys. Lett. **4** (1969) 155.
[18] M. Born, Volumen und Hydratationswaerme der Ionen, Z. Phys. **1** (1920) 45.
[19] M. Antonello *et al.*, Detection of Cherenkov light emission in liquid argon, Nucl. Instr. Meth. in Phys. Res., A 516 (2004) 348.
[20] R. Reininger, U. Asaf, I. T. Steinberger, and S. Basak, Relationship between the energy V0 of the quasi-free-electron and its mobility in fluid argon, krypton, and xenon, Phys. Rev. **B** 28 (1983) 4426.
[21] H. J. Hilke, Detector calibration with lasers - A review, Nucl. Instr. Meth. in Phys. Res. A 252 (1986) 169.
[22] I. Badhrees *et al.*, Measurement of the two-photon absorption cross-section of liquid argon with a time projection chamber, New J. Phys. **12** (2010) 113024, [arXiv:1011.6001 [physics.ins-det]].
[23] A. C. Tam and C. K. N. Patel, Two-photons absorption spectra and cross-section measurements in liquids, Nature Vol. 280 (1979).
[24] C. G. Elles *et al.*, Electronic structure of liquid water from polarization-dependent two-photon absorption spectroscopy, The journal of chemical physics 130 (2009) 084501.
[25] J. Bourotte and B. Sadoulet, Ionization of multiwire proportional chamber gas by double photon absorptio, Nucl. Instr. and Meth. 173 (1980) 463.
[26] G.S. Hurst *et al.*, Resonance ionization spectroscopy and one-atom detection, Rev. Mod. Phy. 51 (4) (1979) 767.